Modeling and Performance Evaluation of a Hysteresis IPM Motor Drive for Electric Submersible Pumps

S. F. Rabbi, SIEEE and M. A. Rahman, LFIEE
Department of Electrical & Computer Engineering
Memorial University of Newfoundland
St. John's, NL, Canada, A1B 3X5
sfr560@mun.ca, arahman@mun.ca

M. M. Sarker, S. D. Butt
Department of Process Engineering
Memorial University of Newfoundland
St. John's, NL, Canada, A1B 3X5
mms426@mun.ca, sdbutt@mun.ca

***Abstract*—This paper presents modeling and analysis of a hysteresis interior permanent magnet (IPM) motor drive for electric submersible pumps. A hysteresis IPM motor can self-start without the need of additional position sensors and complex control techniques. It does not have any slip power losses in the rotor at steady state which results in less heat dissipation and low electrical losses. When used in an electric submersible pump (ESP) for oil production, it has the ability to automatically adapt itself to the changes in well conditions. In this paper, a bond graph model of a hysteresis IPM motor ESP drive is used to predict the effect of rotor dynamics on the transient behavior of the submersible motor drive. Experimental investigations have been also carried out for a laboratory prototype 5HP hysteresis IPM motor drive. Due to increased efficiency and simplified controller requirements, the hysteresis IPM motor is proposed as a replacement for the standard induction motor currently used for downhole ESPs in offshore oil recovery plants.**

Keywords— Electric submersible pump; magnetic hysteresis; modeling; permanent magnet motors; simulation; variable speed drives; performance analysis

I. INTRODUCTION

An oil well contains back pressure at the bottom of it due to the presence of hydrostatic pressure, friction pressure, shut-in surface pressure and other kinetic or potential losses [1]. In order to achieve a desired production rate, an artificial lift method is needed to overcome the bottom-hole pressure of the well. There are several artificial lift techniques are currently available such as gas lift, plunger lift, sucker rod pump, hydraulic jet pump, electric submersible pump (ESP), electric submersible progressive cavity pump (ESPCP), hydraulic piston pump and submersible turbine pump [1-5]. An ESP is an excellent choice to provide artificial lift for offshore petroleum production, and it is the most economical and efficient lift technique based on a cost-per barrel basis [5]. ESPs can produce about 200 to 40000 barrels of fluid per day at various depths from 1000 to over 12000 foot under the sea bed. With the advent of high temperature motors and cables in recent years. ESPs can be deployed to oil wells with temperature above 350^0 F [5]. ESPs are also applicable to both deviated and horizontal wells. It is the most suitable choice for low pressure/low flow wells as the gas lift technique is difficult to apply for such wells. At certain depths (>12000 ft.), an ESP is the best choice for high volume oil production [1-5].

ESPs operate in a downhole hostile environment and experience high temperature, high pressure and the presence of debris. A submersible motor has a unique construction as it has a small diameter (less than a foot) to fit inside the bottomhole tubing string and a long length as much as 100 feet to provide the required horsepower and torque [1]. The diameter of the ESP drive motor is restricted by the outside diameter of the downhole casing which is in between 4 in. to 10 in [1]. As a result, a submersible motor has low inertia. Bottomhole submersible motors are specially designed to withstand high temperature, high mechanical and electrical stress and high inrush torque. Since the inception of electric submersible pumps (ESP), polyphase squirrel-cage rotor water-proof sealed induction motor drives have traditionally been used for ESPs in offshore oil and gas [1-5]. However, induction motors suffer from poor power factor, and poor efficiency because of slip power losses in the rotor. It is also extremely difficult to build an induction motor drive with a longer rotor length and smaller diameter which will meet the power requirement of an ESP. Multi-rotor induction motor is the standard practice for electric submersible pumps. This multi-rotor assembly suffers from frequent failure and shaft breakdowns due to extreme mechanical stress, especially during start-up of the pump. The total intervention cost to replace/repair an ESP unit is very high. It also results in a long downtime for the offshore plant. The average lifetime of an ESP equipped with an induction motor drive is around two years. Due to poor reliability, low lifetime expectancy and very high intervention cost, many offshore petroleum production plants prefer to use other artificial lift techniques such as gas lift, etc. So, improvements in reliability and performance of the ESP can be significant for the offshore oil and gas industries.

In recent years, interior permanent magnet (PM) motor drives have been introduced into electric submersible pump systems by different ESP manufacturers. An IPM motor has high energy density rare earth Neodymium Boron Iron (Nd-B-Fe) permanent magnets embedded inside the rotor for maximum reluctance torque as well as high electric motor torque within minimum volume and weight of the rotor. ESPs equipped with IPM motors driven by sophisticated variable speed drives have been already deployed in few petroleum production plants [2-6]. These ESPs have been found to be superior both in performance and in reliability to the conventional IM driven ESPs. Although a IPM motor is inherently more efficient than an induction motor, it cannot self-start from a fixed frequency balanced 3-phase ac supply [2-4]. The magnets produce braking torque during start which acts as a drag for the rotor. In order to overcome the magnet

brake torque and to produce the required starting torque for the motor, accurate position control of the rotor is required. The standard PM motor drive produces the driving currents for the motor based on the signals received from the external position sensors mounted on the shaft of the rotor. In the case of high speed submersible drives in deep/ultra deep (>10000ft) offshore plants, it may not be possible to synchronize the IPM motor with the supply frequency based on the signals received from thousands of feet under the sea. This may create significant rotor hunting. Relying on the signal received from that distance reduces the reliability of the ESP and can cause possible ESP failures.

This paper investigates the performance analysis of a hysteresis interior permanent magnet (IPM) motor drive for electric submersible pumps. A bond graph model of a hysteresis IPM motor ESP drive has been developed in order to predict its transient rotor dynamic behavior. Simulations have been carried out using the bond graph model to obtain the transient responses of a 5HP 90 gallons per minute (GPM) four-stage 6-inch electric submersible pump drive system. A comparative performance analysis between a hysteresis IPM motor drive and an induction motor drive for the same ESP is presented in this paper. Experimental investigations have been carried on a 3-phase 4-pole 208V 5hp laboratory Mawdsley prototype hysteresis interior permanent magnet motor. Based on the simulation and experimental results, a hysteresis IPM motor drive can self-start without the need of additional position sensors and complex control techniques and it does not have any slip power losses (I^2R losses) in the rotor at steady state. This results in less heat dissipation and high system efficiency. When used in an electric submersible pump (ESP) for oil production, it has the ability to automatically adapt itself to the changes in well conditions. Due to increased efficiency and simplified controller requirements, the hysteresis IPM motor can be a possible replacement for the standard induction motor currently used for downhole ESPs.

II. Electric Submersible Pump

Fig. 1 illustrates the typical arrangement of an offshore petroleum production unit equipped with an electric submersible pump (ESP) system [1]. The ESP is placed close to the bottomhole well inside a narrow tubing string. An electric submersible pump (ESP) is a motor/pump configuration made up of multi-stage centrifugal pumps connected in series in order to provide the required pump head. The interconnected centrifugal pumps are normally driven by a three phase ac motor. The motor is usually controlled by an on-board variable speed drive (VSD). Each stage of the centrifugal pump consists of an impeller and a diffuser. Fig. 2 illustrates the multi-stage centrifugal pump configuration. The exploded view of an ESP is shown in Fig. 3. The fluid from the reservoir travels through the porous media and enters the bottom hole. The fluid enters the pump through an intake. There is a seal section between the pump intake and the motor which prohibits the fluid flowing into the motor. The pump rotates at the same speed as the motor. The fluid first passes through the rotating impeller which adds kinetic energy to the fluid. The fluid leaves through the diffuser which converts the kinetic energy into potential energy, increases the fluid pressure and guides the fluid to the next pump stage. Thus,

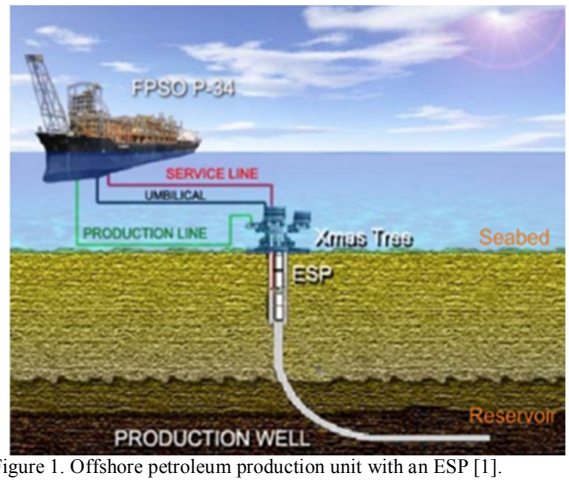

Figure 1. Offshore petroleum production unit with an ESP [1].

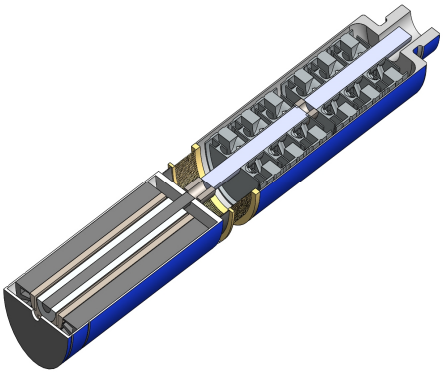
Figure 2. Cross section of a multi-stage ESP.

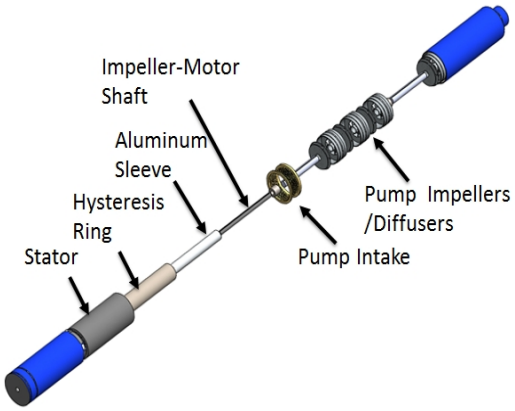

Figure 3. Exploded view of an ESP.

each stage adds enough pressure to the fluid so that it can reach the well head which is attached to the tubing string. The number of pump stages depends on the required pump volumetric flow rate and the head (height) of the pump.

The performance curves of a 5HP 4-stage 6-inch submersible pump are depicted in Fig. 4. The pump is driven by a 3-phase variable speed ac motor drive. The system curve is shown with the red line. The intersection between the system curve and the total dynamic head curve of the pump determines the pump operating point i.e. the pump flow rate and the pump

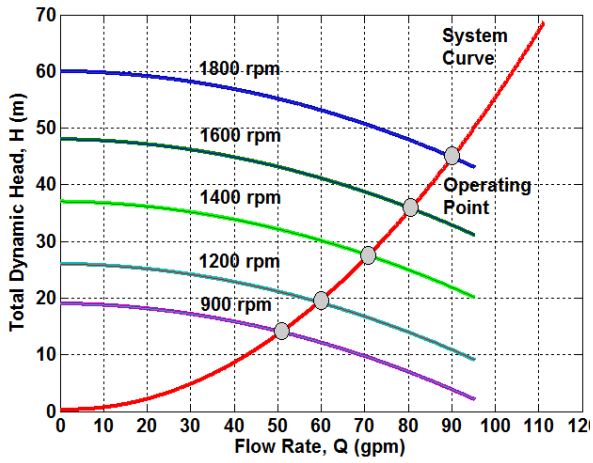

Figure 4. Performance curves of a variable speed ESP drive.

head. The pump can be operated at its best efficiency operating point with the aid of a VSD. The pump volumetric flow rate Q depends on the rotational speed of the impeller and can be expressed as,

$$Q = k_q N_s \tag{1}$$

where k_q is a proportional constant which depends on the impeller geometry and N_s is rotational speed of the impeller in rpm.

The operating head of the pump is calculated from the system curve and is given below,

$$H = k_{h2} Q^2 + k_{h1} Q + H_0 \tag{2}$$

where k_{h2} and k_{h1} are proportional constants and H_0 is the minimum head of the pump.

In a centrifugal pump, the volume of the fluid delivered by the pump against a constant pressure head is proportional to the power of the motor. So, the required load torque for the pump is proportional to the square of the speed of the motor. As a result, the load torque is relatively small at starting. The required mechanical input power to a centrifugal pump is given below [6],

$$P = HQg\frac{1}{\eta} \tag{3}$$

where g is the gravitational acceleration and η is the pump efficiency.

III. Hysteresis IPM Motor Drive

A hysteresis IPM motor's rotor has a cylindrical hysteresis ring made of composite material like 17% or 36% Cobalt-Steel alloy, special Al-Ni-Co, Vicalloy, etc. with high degree of hysteresis energy per unit volume [7-11]. The rare earth permanent magnets are buried inside the hysteresis ring and the ring is supported by a sleeve made of non-magnetic materials like aluminum which forces the flux to flow circumferentially inside the rotor ring [7-11]. Fig. 5 illustrates the rotor of a hysteresis IPM motor. The stator is similar to that of a standard IPM motor. The inclusion of permanent magnets creates rotor saliency without changing the length of the physical airgap and provides an additional permanent source of excitation in the rotor. Fig. 6 presents the slick rotor of a hysteresis IPM submersible motor inside a 6-inch casing. The induced magnetization of the hysteresis material inside the rotor ring always lags behind the time varying magnetic field. This time lag produces the hysteresis motor torque. The maximum starting hysteresis torque depends on the area of B-H loop and the supply frequency. The induced eddy currents in the hysteresis ring generate some additional starting torque called the eddy current torque. The combination of the hysteresis torque and the eddy current torque results in a high torque during starting of a hysteresis IPM motor which overcomes the magnet brake torque [7-11].

The *d-q* axis electrical equivalent circuits of a hysteresis IPM motor in sub-synchronous mode are depicted in Figs. 7 and 8, respectively. The permanent magnet is modeled as a constant current source I_m. Eddy current effect is included in the circuit by modeling it as an equivalent resistance R_e. Hysteresis effect is modeled as an equivalent hysteresis resistance R_h and an equivalent hysteresis inductance L_{hr}. The eddy current torque becomes zero when the motor synchronizes but the hysteresis torque still exists, and the hysteresis ring behaves like a temporarily magnetized permanent magnet. At synchronous operation mode, the hysteresis effect is modeled as a current source, I_{hs} and can be expressed as,

$$I_{hs} = I_s \sin\delta \tag{4}$$

where I_s is the magnitude of the supply current and δ is the hysteresis lag angle between B and H. At steady state

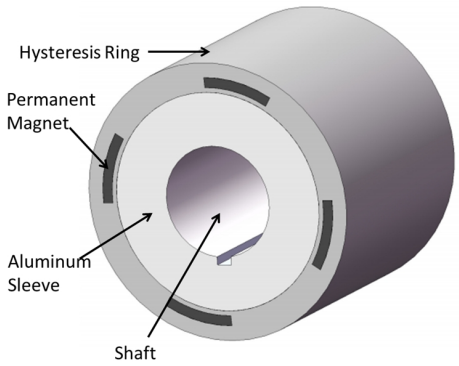

Figure 5. Rotor of a hysteresis IPM motor.

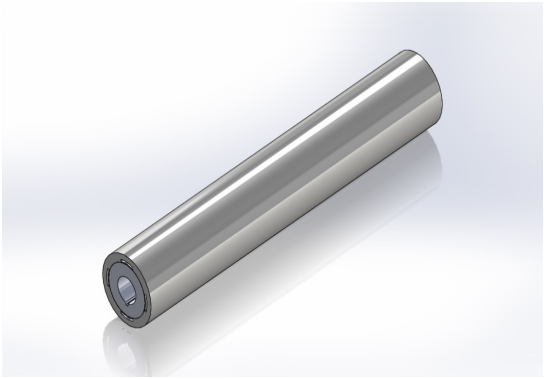

Figure 6. Rotor of a submersible hysteresis IPM motor.

This work was supported by the Natural Sciences and Engineering Research Council of Canada (NSERC).

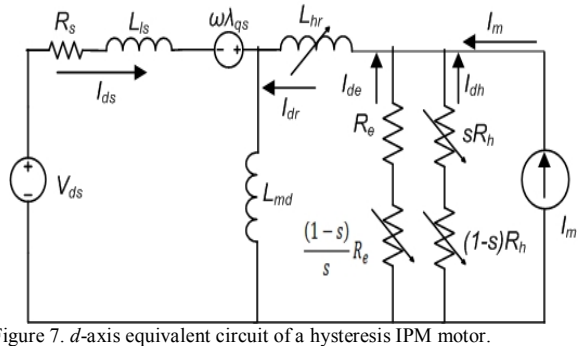

Figure 7. *d*-axis equivalent circuit of a hysteresis IPM motor.

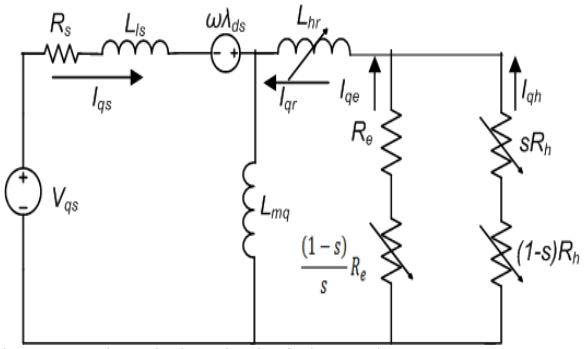

Figure 8. *q*-axis equivalent circuit of a hysteresis IPM motor.

synchronous operation, the excitation is partly provided by the hysteresis current I_{hs} and mainly by the permanent magnet. The insertion of permanent magnets inside the rotor hysteresis ring creates reluctance variation in the air-gap which produces additional reluctance torque. Thus, the starting and synchronizing problems of standards PM motors when supplied directly from line frequency can be solved by the design of a hysteresis interior permanent magnet hybrid rotor.

IV. Bond Graph Modeling of a Hysteresis IPM Submersible Drive

A bond graph is a graphical approach to modeling a dynamic system [12-14]. Bond graphs use a small set of generalized elements to model energy storage, dissipation, boundary conditions, energy transformations and gyrations, and generalized Kirchoff's laws for multiple energy domains. A bond graph is a powerful tool to model a system involving mechanical, electrical, and electromagnetic elements such as the hysteresis interior permanent magnet (IPM) ESP drive system which is proposed in this paper. The word bond graph of a hysteresis IPM ESP drive system is illustrated in Fig. 9. A four stage submersible pump is considered in this paper for simulation. Each stage is represented by a rotating impeller driven by the hysteresis IPM motor. The input and output of each bond graph element is power, which is the product of conjugate generalized effort-and flow variables. Power bonds are labelled with a half arrow. Small "causal strokes" normal to the power bonds indicate whether effort or flow is the output of the adjacent element's constitutive law. The power variables used for the mechanical portion of the simulation are torque, τ and angular velocity, ω. The bond graph model of a hysteresis IPM motor is developed using the equivalent circuits depicted in Figs. 7-8. The inductive coupling between the stator and rotor are considered in the d^r-q^r reference frame rotating with the rotor electrical angular velocity ω_r. The linear relationships between the stator flux linkages and currents, and the rotor flux linkages and currents are represented in terms of self and mutual inductance parameters and these relationships are provided by using the generalized inertia (I) fields in the bond graph [12-14]. Fig. 10 shows the coupling between the stator and rotor state variables.

The electromagnetic torque and the induced voltages are calculated using the equivalent circuit equations of a hysteresis IPM motor [11]. The electromagnetic torque equation of the hysteresis IPM motor contains the flux and current terms. A gyrator structure for the torque and the induced voltages is illustrated in Fig. 11. The modulated gyrator enforces the relations between the electromagnetic torque τ_e and the *d*-*q* axis currents (i_{ds} and i_{qs}) as well as the relation between the induced voltages (e_{ds} and e_{qs}) and the rotor angular speed ω_r.

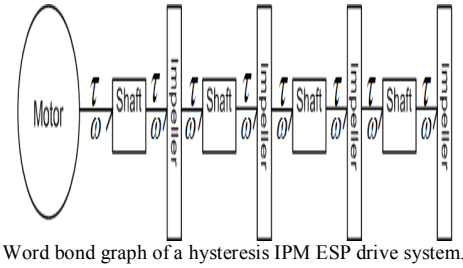

Figure 9. Word bond graph of a hysteresis IPM ESP drive system.

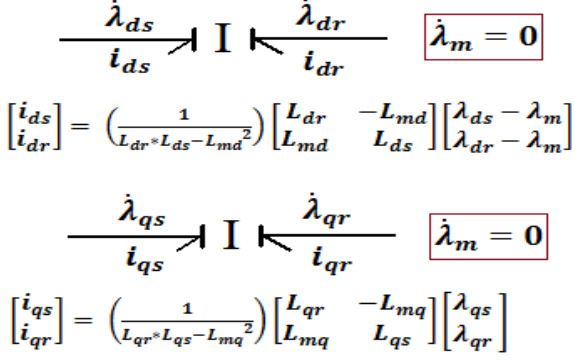

Figure 10. I-field relations and casualties for rotor and stator variables.

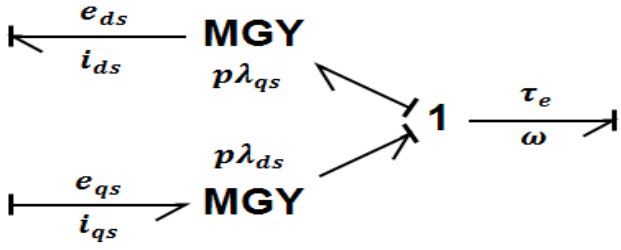

$$e_{ds} = p\lambda_{qs}\omega$$
$$e_{qs} = p\lambda_{ds}\omega$$
$$\tau_e = p(\lambda_{ds} i_{qs} - \lambda_{qs} i_{ds})$$

Figure 11. Gyrator structure for torque and induced voltage.

Fig. 12 presents the complete bond graph model of a hysteresis IPM motor based on its electrical equivalent circuit equations (7-18). Four fluxes (λ_{ds}-λ_m, λ_{dr}-λ_m, λ_{qs} and λ_{qr}) and the angular momentum of the rotor are used as the state variables. Commercial bond graph software is used to automate the generation of state equations. The proposed hysteresis IPM motor model has been driven by a 3-phase fixed frequency balanced ac supply.

A lumped segment approach is used to model the torsional dynamics of the shafts. In the lumped segment approach, the system is divided into a number of elements, interconnected with springs [12-14]. This model is a more cumbersome bond graph representation, and the accuracy of the model depends on the number of elements considered; however, analytic mode shapes and natural frequencies need not to be determined. A total of 4 segments are used for each shaft in the dynamic model. Fig. 13 depicts the torsional dynamic sub-model for a single shaft segment.

The impeller and diffuser of each pump are modeled together as a single lumped inertial body with a fluid viscous damping torque and a load torque. The damping torque and the load torque for the impellers are estimated as $R\omega$ and $R_L\omega^2$, respectively. R and R_L are viscous damping factor and impeller load factor, respectively. The bond graph dynamic model of an impeller is shown in Fig. 14.

V. Simulation Results

Simulations were carried out using 20sim® bond graph modeling software for a 90 GPM 4-stage electric submersible pump driven by a 5 hp, 3-phase, 1800 rpm, 240V hysteresis

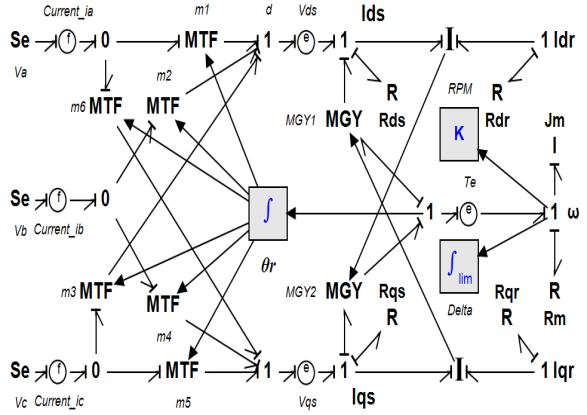

Figure 12. Complete bond graph model of a hysteresis IPM motor.

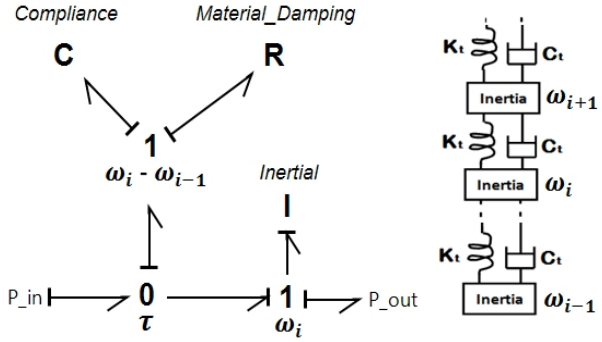

Figure 13. Bond graph torsional model of a shaft segment.

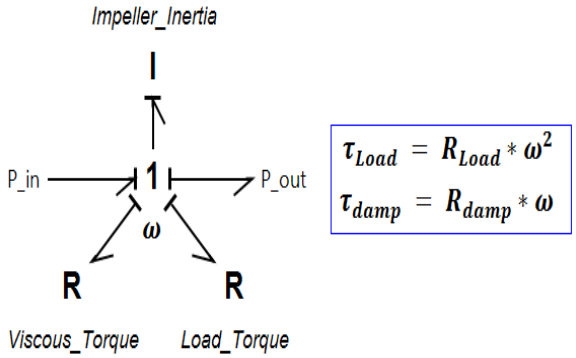

Figure 14. Bond graph torsional model of a shaft segment.

IPM motor drive. Figs. 15a-15b illustrate the performance of the ESP drive for different motor shaft lengths. The motor was loaded at 75% of its rated load. The length of the motor shaft which is connected to the multi-stage pumps is varied from 500mm to 1500mm. The hysteresis IPM motor is started directly from the fixed frequency 60 Hz line supply. Due to its hysteresis ring, the motor generates the starting torque and self-starts by overcoming the magnet brake torque at low speed and ramps up towards the command speed. The motor synchronizes at the command frequency with some speed overshoots and undershoots. These oscillations happen due to the hysteresis phenomenon in the rotor. The hysteresis lag

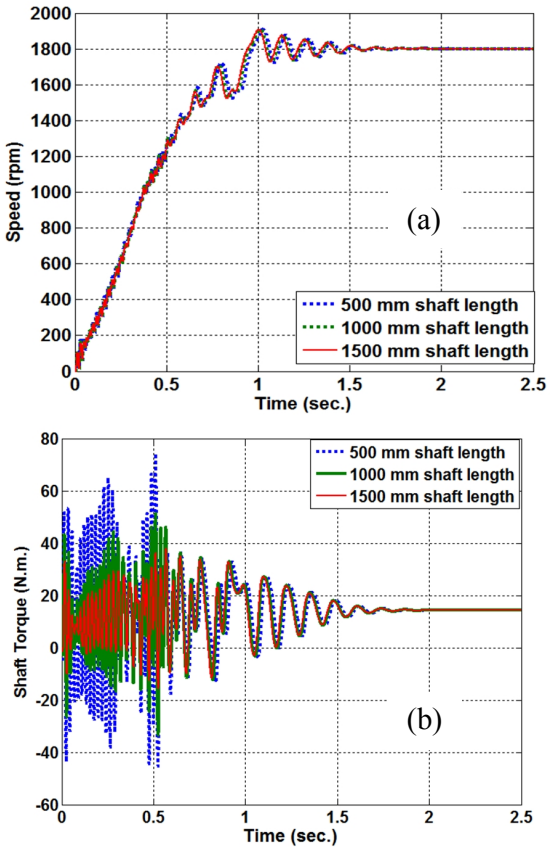

Figure 15. Performance of the ESP drive : (a) speed and (b) torque.

angle goes through some cyclic oscillations before it settles down to a steady state value. It is found that the length of the shaft has negligible impact on the speed response of the motor. The shaft torque response of the hysteresis IPM ESP drive for different shaft lengths is illustrated in Fig. 15b. The developed torque is comprised of an average asynchronous torque and a pulsating torque. The average asynchronous torque combines the hysteresis torque, the eddy current torque and the magnet brake torque. Due to the presence of permanent magnet acting as a current source in the rotor, there is a pulsating torque superimposed on the average asynchronous torque. The pulsating torque assists the motor to a fast acceleration towards the synchronous speed. During the period of synchronization, the torque pulsation dies out and turns into the synchronous torque which is a combination of the magnet alignment torque and the reluctance torque. The magnet brake torque reverses its role and becomes a part of the synchronous torque. As the length of the shaft is increased, the amplitude of the pulsating torque goes down but the frequency of torque pulsations remains the same. This phenomenon is illustrated in Fig. 15b. Thus, as the shaft length increases, the system becomes more damped. Figs. 16a and 16b demonstrate the speed and the torque responses of the ESP drive, respectively for different diameters of the shaft. The length of the shaft and the impeller loads are kept constant at 1000mm long and at the rated load. The magnitude and the frequency of the torque oscillation increase as the diameter of the shaft becomes higher. This also affects the motor run-up responses and reduces the motor's synchronization capability as it takes a longer time to reach the steady state.

The simulated run-up responses of the hysteresis IPM ESP drive for different command frequencies are illustrated in Fig. 17. An adjustable speed drive has been used to soft-start the ESP, and also to limit the inrush current and the starting torque pulsations. The motor starts smoothly during soft-starting and experiences less rotor oscillations. The motor also goes through less speed overshoots and undershoots during synchronization and becomes stable within few seconds. As the inertia of a submersible motor is low, it is a critical requirement for the motor drive to be stabilized within few seconds. The simulated torque responses of motor during soft-starting are depicted in Fig. 18. The magnitude of the starting torque pulsations goes down drastically than it is in the case of direct online start as shown in Figs. 15b-16b. The ESP is operated at its best efficiency point by varying the operating frequency of the motor drive.

The comparative performances of a squirrel cage induction motor (IM) ESP drive system and a hysteresis IPM motor ESP drive system are displayed in Figs. 19a-19d. Both the IM and hysteresis IPM motors are rated as 5 hp 3-phase 1800 rpm 240V, and are supplied from the same 60 Hz balanced ac supply. The impeller load factor is suddenly changed to apply the rated load to the motor as shown in Fig. 19a. As the load changes, the induction motor slows down and the slip becomes almost 3.67%. This results in higher slip losses which in turn increases the temperature of the IM motor, reduces the efficiency of the pump and also reduces the thermal reliability

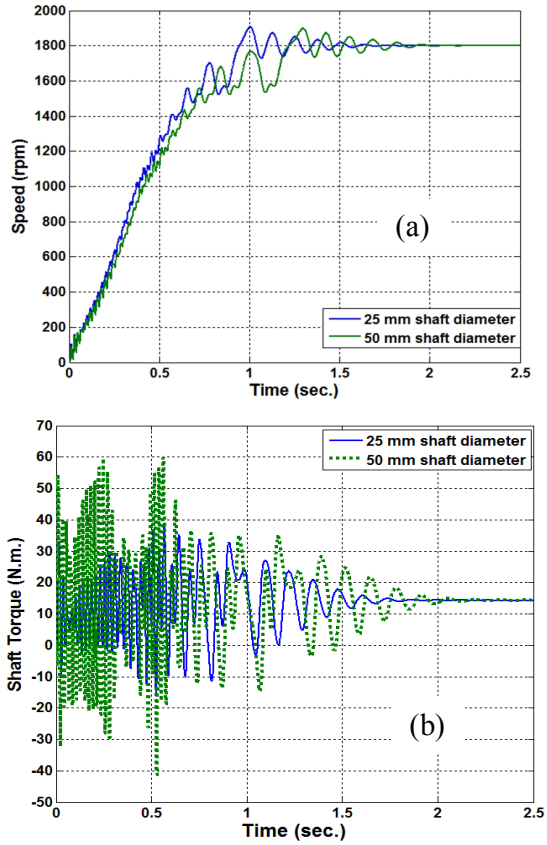

Figure 16. Performance of the ESP drive : (a) speed and (b) torque.

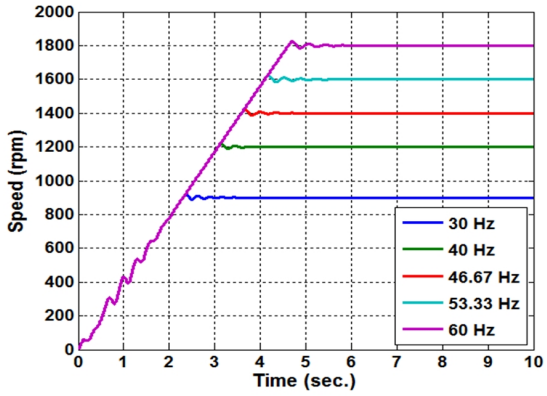

Figure 17. Run-up performances of a variable speed ESP motor drive.

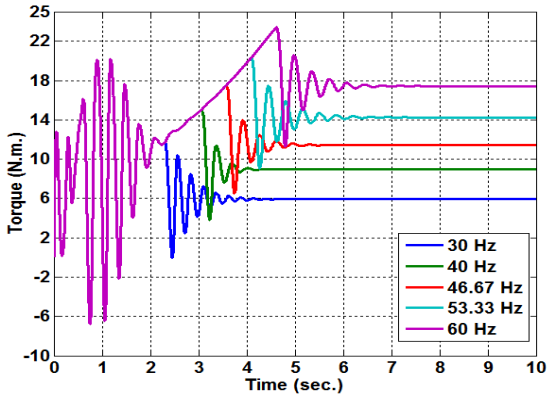

Figure 18. Torque responses of a variable speed ESP motor drive.

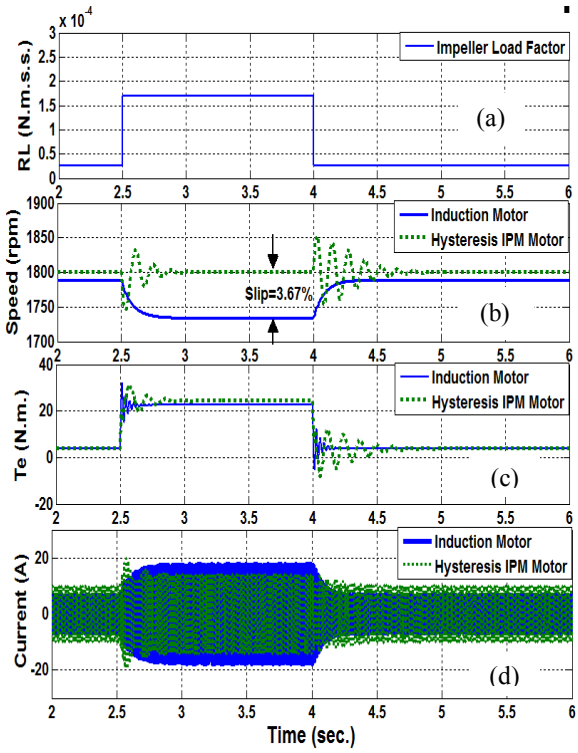

Figure 19. Comparative performances between an IM ESP drive and a hysteresis IPM motor ESP drive: (a) Impeller load factor, (b) speed, (c) torque and (d) line current.

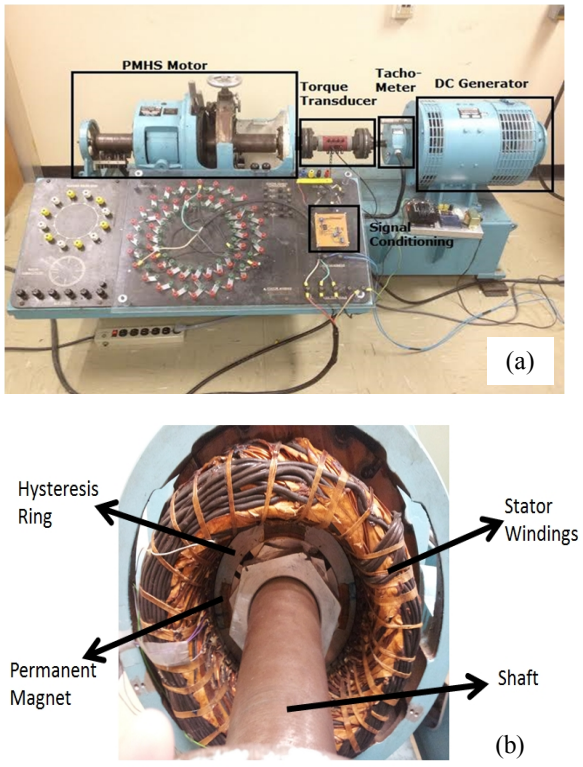

Figure 20. Experimental set-up: (a) system set-up and (b) laboratory prototype of a hysteresis IPM motor.

of the ESP. However, in the case of hysteresis IPM motor, the speed remains the same as the magnets produce the necessary excitation current to remain at the synchronous speed. Figs. 19b and 19c demonstrate the speed and torque responses, respectively of the IM and hysteresis IPM motor ESP drive system for sudden change in load torque. The input phase current of the IM drive and hysteresis IPM motor drive are shown in Fig. 19d. The IM draws more current from the line than the hysteresis IPM motor as the load increases. As a result, a hysteresis IPM motor ESP drive has a higher efficiency at full-load than that of an IM ESP drive.

VI. Experimental Results

The experimental testing has been performed on a Mawdsley generalized machine. The stator is rated at 3-phase 4-pole 208V with delta connected double layer windings. The rotor of the Mawdsley machine is replaced by a 36% Cobalt-Steel hysteresis IPM rotor with Nd-B-Fe magnets. The block diagram of the overall system set-up is displayed in Fig. 20a. Fig. 20b displays an experimental laboratory prototype of the hysteresis IPM motor. The motor is lightly loaded by a dc generator. The motor is soft-started with an adjustable speed drive. In order to observe the effect of the rotor shaft geometry on the motor run-up performances, the shaft of the rotor is extended to 1000 mm and the diameter of the shaft is chosen to be 50mm.

The run-up performance of the motor at 60 Hz and 50Hz command frequencies are illustrated in Figs. 21a and 21b, respectively. The motor has a smooth start and ramps up

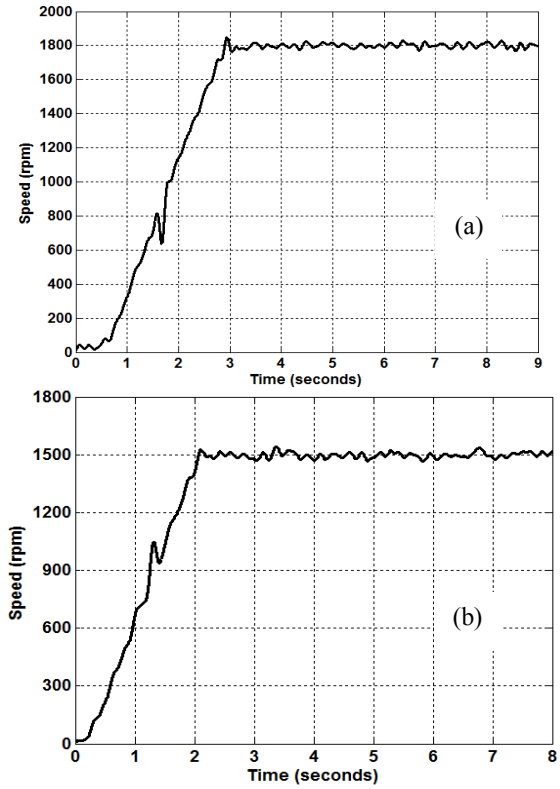

Figure 21. Experimental run-up responses of a hysteresis IPM motor : (a) 60 Hz and (b) 50 Hz.

towards the synchronous speed. Due to the presence of torque pulsations, there are few speed reversals in the run-up response of the motor. There is no significant mechanical vibration during the start-up. The synchronization process starts at 3 sec and the motor synchronizes with few speed overshoots and undershoots within few seconds. The instantaneous torque waveform is presented in Fig. 22. The instantaneous torque rises gradually and helps the motor reach close to the synchronous speed. There exists pulsating torque superimposed on the total hysteresis and eddy current torque which results in torque reversals in the instantaneous torque curve. During the synchronization process, the frequency and the magnitude of the torque pulsation die out slowly and the pulsating torque becomes a part of the total synchronous torque. The line current waveform of the inverter is shown in Fig. 23. The motor starts with a low starting current which reduces the electrical stress on the inverter.

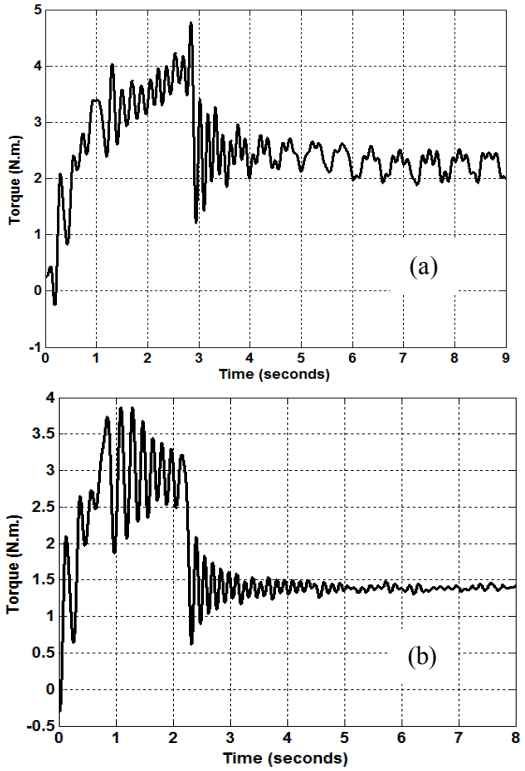

Figure 22. Experimental torque responses of a hysteresis IPM motor : (a) 60 Hz and (b) 50 Hz.

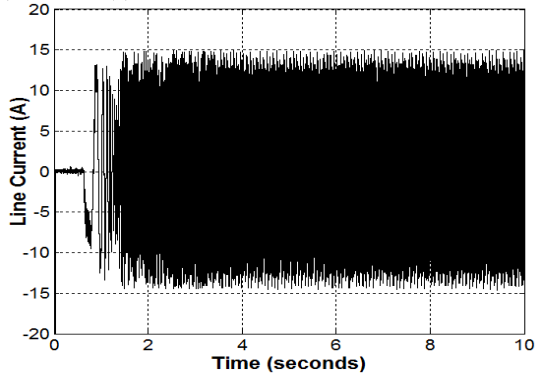

Figure 23. Experimental line current of the motor at 60 Hz.

VII. CONCLUSION

This paper presents the modeling and dynamic performance analysis of a hysteresis interior permanent magnet (IPM) electric submersible pump (ESP) drive system. A bond graph model of the dynamic system is developed and presented in this paper. Simulations are carried out to obtain the transient and steady state responses of a 5 hp 90 GPM hysteresis IPM ESP drive system. A comparative performance analysis between an induction motor ESP drive system and a hysteresis IPM ESP drive system is presented and explained in this paper. Experimental investigations have been carried on a laboratory prototype hysteresis IPM motor. Based on the simulation and experimental results, a hysteresis IPM motor drive is found superior, and has the potential to improve the performance and the reliability of the standard ESP drive systems in harsh offshore environment.

REFERENCES

[1] O. J. Romero and A. Hupp, "Subsea electrical submersible pump significance in petroleum offshore production," *ASME Journal of Energy Resources Technology,* vol. 136, no. 1, pp. 012902, September 2014.

[2] T. R. Brinner, R. H. McCoy and T. Kopecky, "Induction versus permanent-magnet motors for electric submersible pump field and laboratory comparisons," *IEEE Transactions on Industry Applications,* vol. 50, no.1, pp. 174-181, January 2014.

[3] M. S. Dillard and D. T. Greiner, "Transient voltage protection for induction motors including electrical submersible pumps," *IEEE Transactions on Industry Applications,* Vol. 23, No.2, pp. 365-370, March 1987.

[4] V. Pavlenko, "Permanent magnet synchronous motor (PMSM)-new type of drives for submersible oil pumps", *Proceeding of the 2008 SPE Russian Oil & Gas Technical Conference and Exhibition*, Moscow, Russia, October 28-30, 2008.

[5] J. F. Lea and H. V. Nickens, "Selection of artifical lift", *Proceeding of the SPE Mid-Continent Operations Symposium,* Oklahoma City, Oklahoma, USA, March 28-31, 1999.

[6] T. Ding, N. Takorabet, F.M. Sargos and X. Wang,, "Design and analysis of different line-start PM synchronous motors for oil-pump applications", *IEEE Transactions on Magnetics, Vol. 45, No. 3, pp.* 1816–1819, 2009.

[7] K. Kurihara and M. A. Rahman, "Transient performance analysis for permanent-magnet hysteresis synchronous motor," *IEEE Transactions on Industry Applications*, Vol. 40, No. 1, pp. 135–142, January 2004.

[8] J. J. Nitao, E. T. Scharlemann and B. A. Kirkendall, "Equivalent Circuit Modeling of Hysteresis Motors", Lawerence Livermore National Laboratory , pp. 1-52, July 2009

[9] M. A. Rahman and R. Qin., "Starting and Synchronization of Permanent Magnet Hysteresis Motors", *IEEE Transactions on Industry Applications*, Vol. 32, No. 5, pp. 1183-1189, September 1996.

[10] J. Qian and M. A. Rahman, "Analysis of field oriented control for permanent magnet hysteresis synchronous motors", *IEEE Transactions on Industry Applications*, Vol. 29, No. 6, pp. 1156-1163, Nov. 1993.

[11] S. F. Rabbi and M. A. Rahman, "Transient analysis of a line start hysteresis interior permanent magnet motor", *Proc. 6th IEEE Energy Conversion Congress and Exposition (ECCE),* Pittsburgh, PA, USA, May 4-7, 2014, p. 4866-4873.

[12] D. C. Karnopp, D. L. Margolis and R. C. Rosenberg, *System Dynamics:A Unified Approach*, Wiley, New York, 1990.

[13] D. G. Rideout. J. L. Stein and L. S. Louca. "Systematic Assessment of Rigid Internal Combustion Engine Dynamic Coupling." *J. Eng. for Gas Turbines and Power*, Vol. 130, pp. 022804, 2008.

[14] D. C. Karnoop, "Understanding Induction Motor State Equations Using Bond Graphs", *Proceedings of the International Conference on Bond Graph Modeling and Simulation*, Orlando, Florida, USA, 2008.